



OPEN

Synthesis, spectroscopic characterization techniques of aromatic iminoaniline derived compound, along with the evaluation of its LNO properties using quantum chemistry

R. Chadli^{1,2✉}, M Zouaoui Rabah^{2,3}, I. Khelladi⁴, A. Haddou⁴, B. Ameri⁵ & M. Sakkal-Rahal⁴

In this research work, we synthesized a Schiff base derivative, *N,N*-dimethyl-4-[[[(4-nitrophenyl)imino]-methyl]aniline, denoted as (n1). The molecule (n1) was characterized using spectroscopic analyses, including FT-IR, NMR ¹H, and ¹³C. Our compound (n1) is an unsaturated molecule, consisting of two benzylic rings connected by a methylimine bridge. The resulting system comprises seven alternating π bonds. At both ends of (n1) and in the para position, there are the $N(CH_3)_2$ group with a strong electron-donating effect and the NO_2 group with a strong electron-accepting effect. The molecular structure of our compound prompted us to evaluate and study its properties in the field of NLO. The assessment of NLO properties is conducted by determining the E_{gap} and employing density functional theory (DFT) quantum chemistry studies. The optical gap of (n1), measured using the Tauc method, is found to be 2.7 eV, serving as a reference value for the choice of the DFT functional in theoretical calculations. Quantum chemistry studies were carried out using Gaussian09 software, and the results were visualized with GaussView05. CAM-B3lyp functional was chosen for theoretical calculations due to its close agreement with experimental values. The studies confirm that (n1) exhibits significant NLO properties. Additionally, NBO (Natural Bond Orbital) analyses provide insight into the mechanism and trajectory of intramolecular charge transfer in (n1).

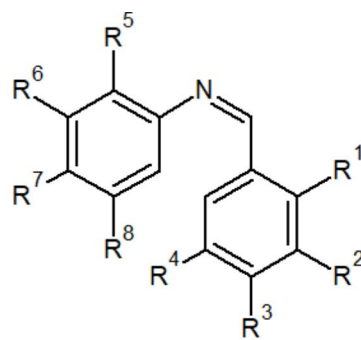
Keywords Dimethylaminobenzaldehyde, Energy gap, Non-linear optics, DFT, MBO

The extensive use and utilization of laser devices in various fields such as industry¹, medicine², scientific research, computing, and communications^{3,4}, there is a growing need to explore new materials possessing nonlinear optical properties. These materials can serve as optical limiters to protect against laser radiation⁵ or act as reactors to modify laser wavelengths. Unsaturated organic materials containing π bonds, in an alternative fashion, stand among the prime candidates due to their rapid light response, flexibility, and high damage thresholds. Within this category, derivatives of diphenylmethanimine are notable, as they link two benzyl cycles, one of which carries an electron-donating group such as (CH_3 , NH_2 , $N(C_2H_5)_2$...) and the other carries an electron-attracting group such as (NO_2 , CN , Cl).

Experimental and theoretical studies have confirmed that these organic compounds, specifically imines, possess intriguing nonlinear optical properties, making them promising candidates for applications in the laser field. Imine compounds are straightforward to synthesize, resulting from the direct action of aldehyde functions

¹Laboratoire de Chimie Physique, Organique et Macromoléculaire, Faculty of Exact Sciences, University Djillali Liabes of Sidi Bel-Abbes, B.P. 89, Sidi Bel Abbès 22000, Algeria. ²Laboratory of Materials Chemistry Catalysis and Reactivity, Department of Chemistry, Faculty of Exact Sciences and Informatics, Hassiba BenBouali University, Chlef, P.O. Box 78C, Ouled Fares Chlef 02180, Algeria. ³National Polytechnic School of Oran, Oran 31000, Algeria.

⁴Laboratoire de Chimie Théorique de Bio- et Nanosystemes, Faculty of Exact Sciences, University Djillali Liabes of Sidi Bel-Abbes, B.P. 89, Sidi Bel Abbès 22000, Algeria. ⁵Laboratoire de Physico-Chimie des Matériaux Avancés, Faculty of Exact Sciences, University Djillali Liabes of Sidi Bel-Abbes, B.P. 89, Sidi Bel Abbès 22000, Algeria. ✉email: mailchadli@yahoo.fr



Reference	Compound
[10]	$R^1=R^2=R^4=R^5=R^7=R^8=H$, $R^3=N(CH_3)_2$ and $R^6=Cl$
[11]	$R^1=R^2=R^4=R^6=R^7=R^8=H$, $R^3=NO_2$ and $R^5=Cl$
[12]	$R^1=R^2=R^4=R^6=R^7=R^8=H$, $R^3=NO_2$ and $R^5=OCH_3$
[13]	$R^1=R^3=R^4=R^5=R^6=H$, $R^2=OH$, $R^7=CH_3$ and $R^8=NO_2$
[14]	$R^3=R^4=R^6=R^7=R^8=H$, $R^1=R^2=CH_3$ and $R^5=Cl$
[15]	$R^1=R^2=R^3=R^6=R^8=H$, $R^4=OH$ and $R^5=R^7=NO_2$
	$R^1=R^2=R^3=R^6=R^8=H$, $R^4=OH$, $R^5=CH_3$ and $R^7=NO_2$

Fig. 1. Structure of some active imines in NLO published recently.

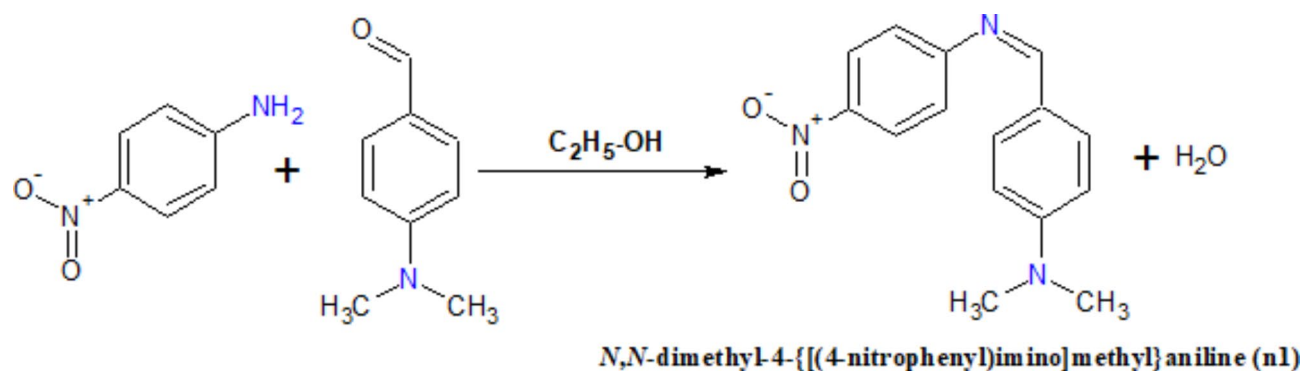


Fig. 2. Synthesis of compound (n1).

on amine functions. The synthesis efficiency is notably high, and these compounds are known for their stability with narrow energy band gaps^{6–9}. They are often employed in second-order generation processes.

In this article, we shed light on one of the new organic compounds derived from diphenylmethanimine, namely *N,N*-dimethyl-4-[[[(4-nitrophenyl)imino]methyl]aniline, designated as (n1). This new compound, n1, is considered as a promising compound in the NLO field, in terms of chemical structure and electronic properties, by comparing with many same compounds of imine family published recently, presented in Fig. 1 below, which have proven their efficiency and importance in the nonlinear optical field. But most of these compounds did not combine the two elements NO_2 and $N(CH_3)_2$ in the same molecule. In this research work, we have proven the validity of our expectations through the results obtained, which designate the compound n1 as one of the most promising organic compounds in the field of NLO. In addition, the low value of E_g makes it a very efficient molecule in inorganic synthesis and complexes in coordination chemistry, which is no less important than the field of NLO.

The compound n1 was synthesized through a reaction between *p*-dimethylaminobenzaldehyde and *p*-nitroaniline in an alcoholic solution. Compound (n1) was synthesized with a yield of over 68%. Figure 2 illustrates the synthesis reaction, the molecular formulas of the reactants, and the obtained molecular structure of (n1).

To confirm the molecular structure of our compound (n1), we conducted infrared spectroscopic (FT-IR) and nuclear magnetic resonance (NMR) analyses, including NMR 1H and NMR ^{13}C . The FT-IR analysis of compound (n1) clearly reveals the presence of characteristic bands for aromatic hydrogens at around 3020 cm^{-1} , the methyl group at around 2850 cm^{-1} , and the imine group at approximately 1635 cm^{-1} . By comparing the spectra of the resulting compound with those of the reactants, we observed the disappearance of the 1640 cm^{-1} band, indicative of the carbonyl group, as well as the disappearance of the two bands at 3250 and 3115 cm^{-1} , signifying the primary amine. Simultaneously, we noted the emergence of the 1635 cm^{-1} band, indicating the presence of the imine function.

Figure 3 presents the 1H NMR spectrum, clearly illustrating the presence of aromatic hydrogens in the chemical shift range from 6.62 to 8.28 ppm. The imine hydrogen, labeled as H6, is observed at 9.75 ppm, and the presence of two methyl groups is confirmed by the singular chemical shift at 3.10 ppm.

Following the synthesis of compound (n1) and the confirmation of its molecular structure, theoretical DFT (Density Functional Theory) and experimental studies were conducted to elucidate its nonlinear optical properties. The results of these investigations will be presented in the subsequent sections of this article.

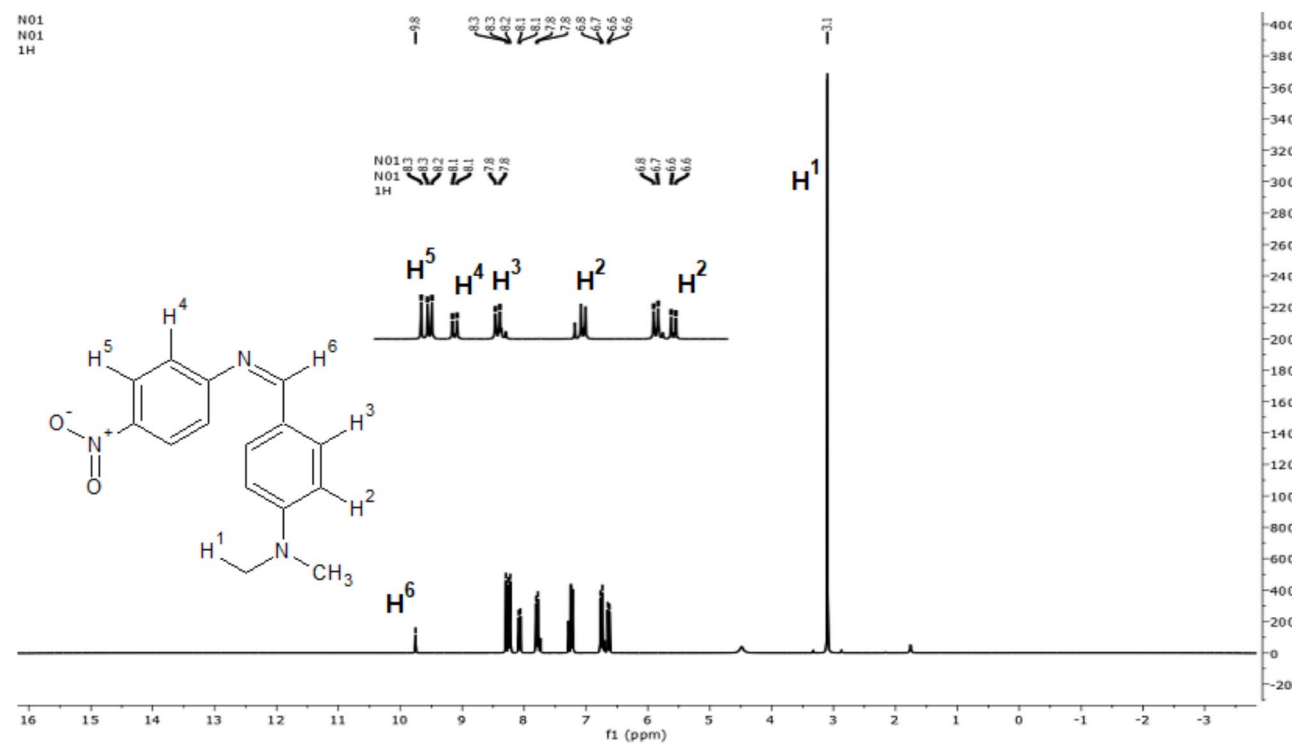


Fig. 3. ¹H NMR spectrum of compound (n1).

Materials and methods

The products and solvents used in the synthesis of (n1) were of Riedel-de Haën brand. The spectroscopic equipment utilized for the analyses included the following: Laboratory Materials and Catalysis FT-IR Spectrophotometer: Perkin Elmer Spectrum Two. UV-Visible Double-Beam Spectrophotometer: Shimadzu UV-2401, located at the Measurement Center of the Department of Chemistry, Faculty of Exact Sciences, University Djillali Liabes, Sidi Bel Abbès and Varian MercuryPlus 300 MHz Spectrometer: Located at the Applied Organic Synthesis Laboratory (LSOA), University Oran1 Ahmed Ben Bella.

Synthesis of (n1)

In an oil bath, a 250 mL round-bottom flask equipped with a reflux condenser and a small magnetic stirring bar was used. 1.38 g (10 mmol) of 4-nitroaniline and 30 mL of alcohol were added to the flask. The mixture was stirred until complete dissolution. In an addition funnel, an alcoholic solution was prepared by dissolving 1.49 g (10 mmol) of 4-dimethylaminobenzaldehyde in 10 mL of ethanol. At room temperature and under stirring, the content of the addition funnel was added dropwise to the flask. The reaction mixture was refluxed for two hours. At the end, the flask was placed in an ice bath with 50 mL of cold water for cooling and precipitation of the imine (n1). The formed imine (n1) was filtered and then dried in open air. Recrystallization of (n1) was carried out in a methanol/chloroform mixture (5/1, v/v). The final product was obtained with a mass of 1.82 g and a yield of 68.5%.

(n1) is an orange powder with a melting point (mp) of 138 °C. IR (ν, cm⁻¹): 3094 et 3027 (H-Ar); 2850–2927 (CH₃); 1600 (C=C); 1575 et 1370 (NO₂); 1230 et 1204 (H₃C-N); 1100 et 1163 (C-N). ¹H RMN (300 MHz, CDCl₃, δ, ppm): 9.8 (1H, s, H₆-C=N); 8.29–8.22 (2H, d, H₅); 8.09–8.06 (2H, d, H₄); 7.81–7.74 (2H, dd, H₃); 6.77–6.62 (2H, m, H₂); 3.10 (6H, s, N(CH₃)₂, H₁). ¹³C RMN (300 MHz, CDCl₃, δ, ppm): 162.18; 158.99; 153.15; 152.64; 144.71; 131.23; 125.69; 121.41; 111.97. The spectroscopic analysis results obtained are in good agreement with those reported in the literature¹⁶.

Electronic absorptions

Electronic absorption spectroscopic analyses were performed using a spectrophotometer, scanning from 190 to 1100 nm. Scanning beyond the wavelength value of 425 nm did not reveal any electronic absorption. Chloroform was chosen as the solvent.

The results obtained from UV-Vis spectroscopy are illustrated in Fig. 4, where the Fig. depicts the variation of absorbance as a function of wavelength for compound (n1) dissolved in chloroform. From the curve, it is evident that there is a high absorbance corresponding to a wavelength of 338 nm, which represents $n \rightarrow \pi^*$ transitions occurring within the benzyl cycles, nitro group, and amine group. Additionally, a weak absorption at 242 nm is observed, representing $\pi \rightarrow \pi^*$ transitions due to the presence of π bonds. In the visible spectrum, very low absorbance is observed from 425 nm to 800 nm, indicating high transparency of the solution in the visible light range. These results will be utilized in further studies on the nonlinear optical properties of compound (n1)¹⁷.

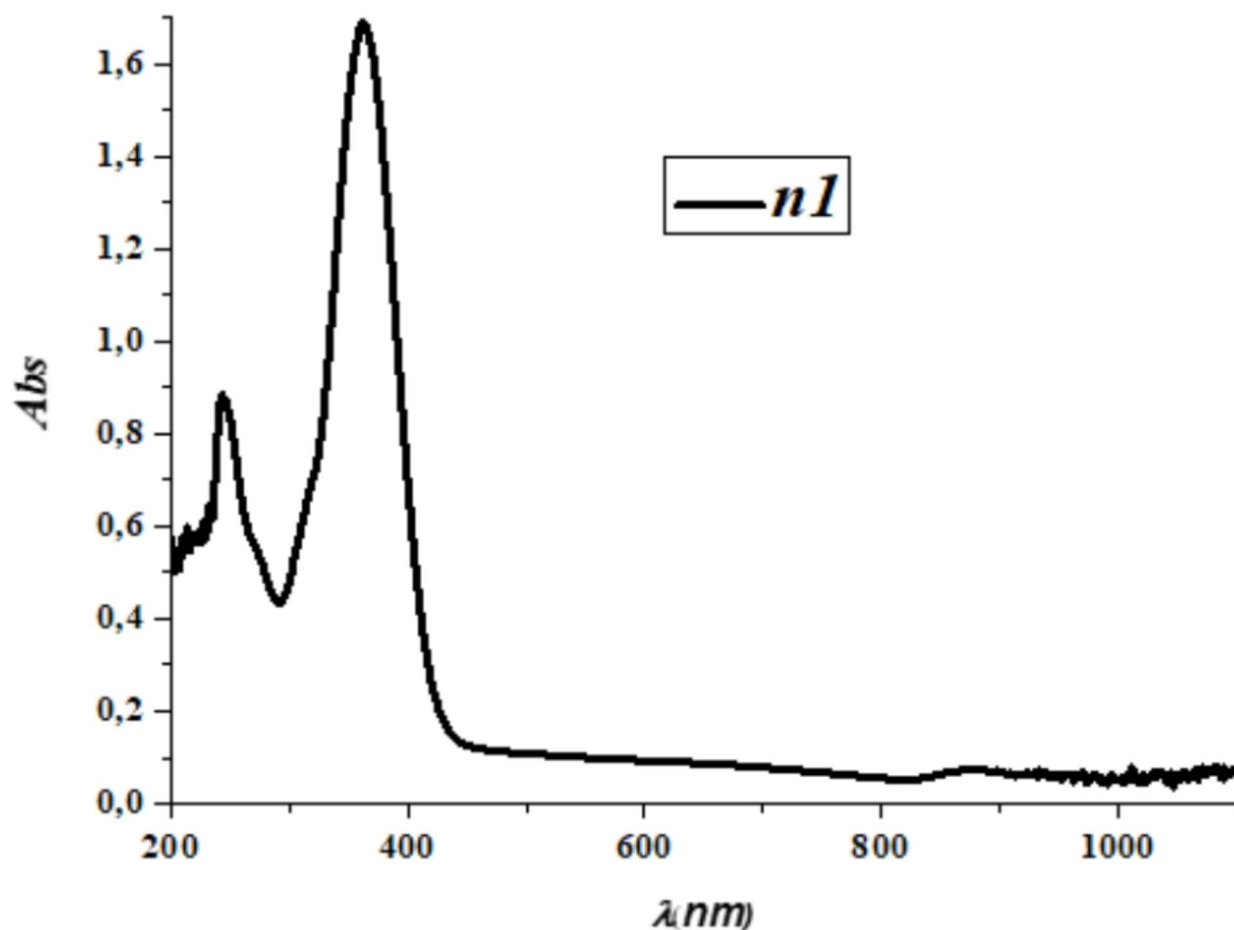


Fig. 4. UV-Vis spectrum of (n1).

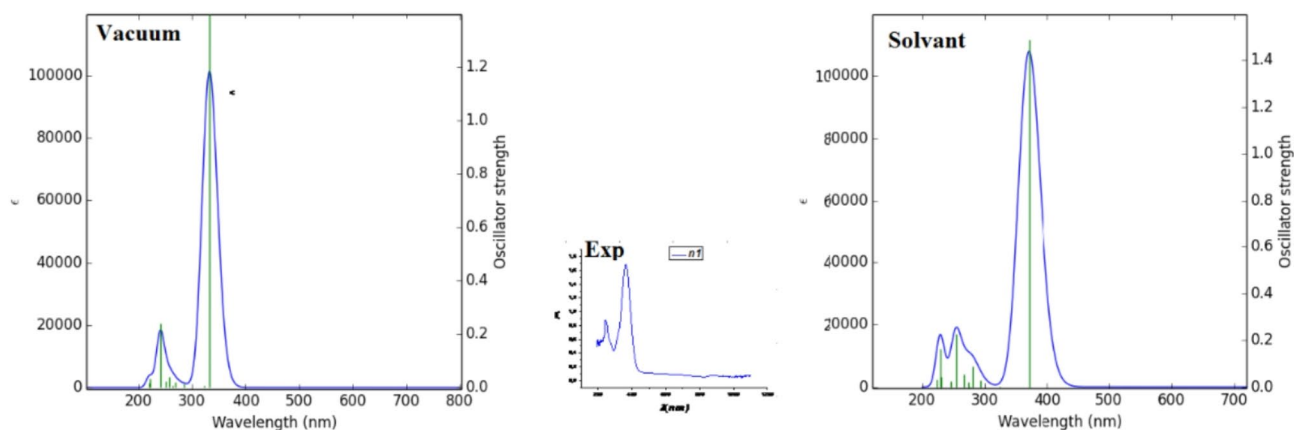


Fig. 5. Wavelengths λ in nm of the molecule (N1) in gaseous state and in solvent presence using the implicit solvation model PCM calculated by TDA-CAM-B3LYP /6-311g(d,p) compare with experimental.

Electronic absorptions theoretical and experimental

The excited states of the molecule (n1) in the specific solvent (Chloroform) were determined by time-dependent functional density theory TD-DFT in particular TDA-CAM-B3LYP /6-311g++(d,p) compare with experimental. The results are shown in Fig. 5.

Examining Fig. 5: for the molecule (n1), it is remarkable that both theoretical curves show overall two majority bands similar to the experimental one. The UV-Vis spectrum curve in the presence of solvent is slightly

more intense, determined by a high extinction coefficient (ϵ) and a wavelength (λ) higher by around 370 nm, indicating a transition of $n \rightarrow \pi^*$ nature. In vacuum, on the other hand, the curve is characterized by a slightly lower ϵ and a rather low λ of around 332 nm, indicating a transition of nature $\pi \rightarrow \pi^*$. Furthermore, the value of λ_{max} in the presence of solvent is higher than that found in the gas phase, indicating a shift of the intense band towards higher wavelengths with increasing intensity. This demonstrates that our solvent has a bathochromic effect. What's more, the λ_{max} obtained for our molecule in solvent and vacuum are in the transparent region of the Near UV, which is essential for making transparent films active in NLO.

X-ray diffraction analysis

The powder of the compound **n1** sample structural was analysis by powder X-ray diffraction. The model of X-ray diffractometer used is Rigaku "MiniFlex 600". The X-ray tube operated with $\text{CuK}\alpha_1$ ($\lambda = 1540.6 \text{ m}\text{\AA}$). Data were captured and recorded by scanning 2θ values between 3° and 90° at room temperature. The XRD analysis data of our compound **n1** are examined with the MATCH!3 software by used of Rietveld refinement method. The different major diffraction peaks most characteristic of the crystalline nature of the **n1** obtained are well presented in the Fig. 6. The DRX data of (**n1**) obtained favor the monoclinic crystal form.

Computational calculations

All theoretical calculations based on quantum chemistry were performed using the Gaussian09 program¹⁸ and the results were analyzed with the Gaussview5.0 visualization program¹⁹. The geometry of the ground state of the molecule (**n1**) shown in Fig. 6 in the gas phase was optimized using the density functional theory (DFT) method. No particular selection of functionals was made, only the B3LYP functional with the basis set 6-31G++(d,p)²⁰ was chosen as it is often used and considered practical and reasonable for obtaining theoretical results close to experimental data, particularly in X-ray diffraction, the choice of basis was taken from previous work. Based on the optimized geometry, a frequency calculation was performed to verify that this structure is really a minima. Single point (SP) calculations were performed on this structure using the following long separation functionals: CAM-B3LYP, LC-wPBE, LC-BLYP, M11, and the M06-2X functional, in order to obtain the appropriate functional for the experimental results. On the basis of the chosen functional combined with the base 6-311G++(d,p) we performed calculations on the electronic parameters in particular the energy gap $\Delta E_{(\text{Homo-Lumo})}$, the most occupied molecular orbital (HOMO) and the least occupied (LUMO) which are used to calculate chemical reactivity descriptors (appendix 1). The excited states of the molecule (**n1**) in the specific solvent (Chloroform) were determined by time-dependent functional density theory TD-DFT²¹. An analysis based on the NBO approach, which gives an explanation of the amount of charge transferred within the molecule (TCI) linked to the parameter to obtain the delocalization energy $E(2)$ representing the interactions

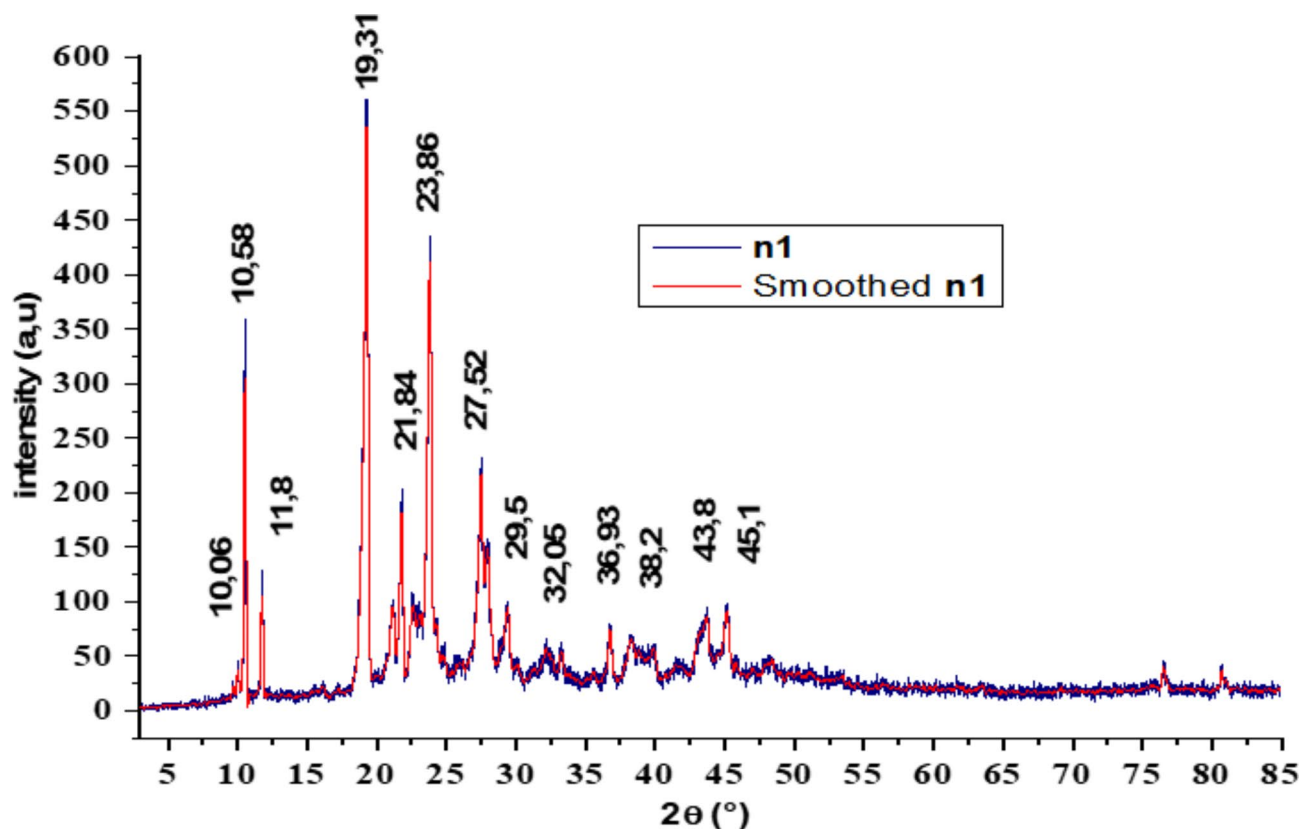


Fig. 6. UV-Vis spectrum of (**n1**).

between the donor (D) and acceptor (A) on a well-defined trajectory of the free doublet from (D) to (A). The linear optical (LO) and non-linear optical (NLO) properties summarized by the parameters of the static anisotropic polarizabilities (α) and the static (in the absence of an electric field) quadratic hyperpolarizabilities (when $\lambda=\infty$ (0 eV)), and dynamic (when frequency $\omega \neq 0$) calculated at CAM-B3LYP combined with the above basis and second harmonic generation (SHG) is elaborated at different wavelengths. Generally, experimental investigations concern $\omega=0.25$ eV; 0.50 eV; 0.65 eV and 1.17 eV, corresponding respectively to the wavelength values $\lambda=4959$ nm, 2479 nm, 1907 nm and 1064 nm. Let's finalize our study with an Analysis of the excited states of our molecule with a comparative study between different acceptors by the NBO method. The global reactivity parameters calculated in this section are: Dipole moment (μ), electron affinity (A), ionization energy (I), overall hardness (η), chemical potential (μ), overall electronegativity (χ), overall electrophilicity index (ω). In addition, other parameters were calculated such as: dipole moment μ_{tot} , energy gaps (ΔE_{H-L}) and charge transfers (β_{ct}), static and dynamic polarizability and hyperpolarizabilities as well as excited state parameters summarized by maximum wavelengths λ_{max} , oscillator strengths (f), percent excitations (%) (Fig. 7).

$$I = -E_{HOMO} \quad (1)$$

$$\sigma = \frac{1}{\eta} \quad (2)$$

$$A = -E_{LUMO} \quad (3)$$

$$\eta = I - A \quad (4)$$

$$\chi = \frac{I + A}{2} \quad (5)$$

$$\mu = -\chi \quad (6)$$

$$\omega = \frac{\mu^2}{2\eta} \quad (7)$$

$$\beta_{CT} = \frac{-\mu}{\eta} \quad (8)$$

$$\mu_{tot} = \sqrt{(\mu_x^2 + \mu_y^2 + \mu_z^2)} \quad (9)$$

$$\alpha = \frac{1}{3}(\alpha_{xx} + \alpha_{yy} + \alpha_{zz}) \quad (10)$$

$$\Delta\alpha = \sqrt{\frac{((a_{xx} - a_{yy})^2 + (a_{yy} - a_{zz})^2 + (a_{zz} - a_{xx})^2) + 6(a_{xx}^2 + a_{yy}^2 + a_{zz}^2)}{2}} \quad (11)$$

$$\beta_{tot} = \frac{5}{3} \sqrt{(\beta_x^2 + \beta_y^2 + \beta_z^2)} = \frac{5}{3} \beta_0 \quad (12)$$

$$\beta_x = (\beta_{xxx} + \beta_{xyy} + \beta_{xzz}) \quad (13)$$

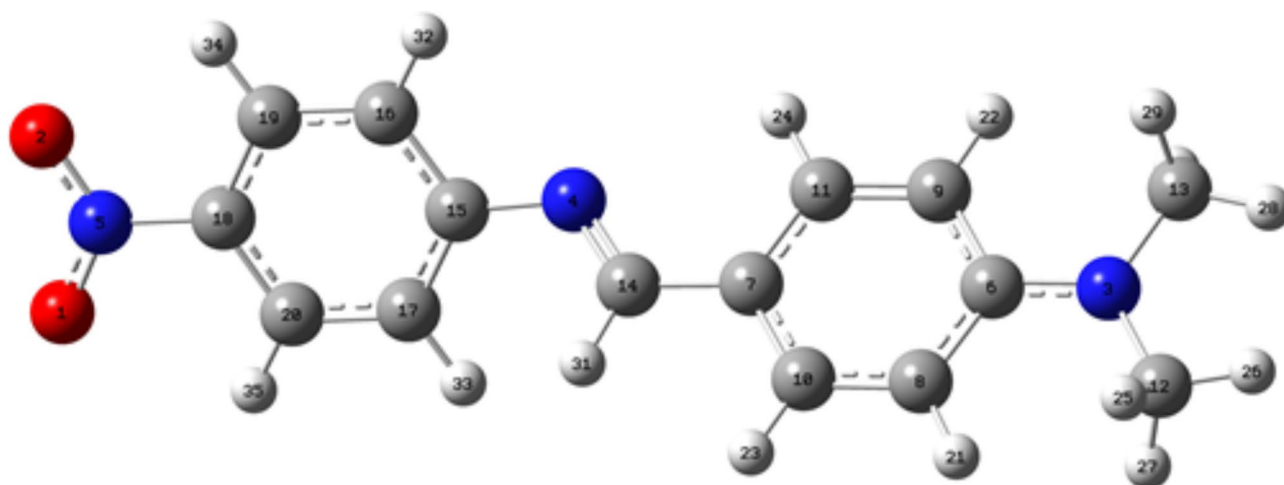


Fig. 7. Structure of the molecule (n1).

$$\beta_y = (\beta_{xxy} + \beta_{yyy} + \beta_{yzz}) \quad (14)$$

$$\beta_z = (\beta_{xxz} + \beta_{yyz} + \beta_{zzz}) \quad (15)$$

$$\gamma = \frac{1}{5} (\gamma_{xxx} + \gamma_{yyy} + \gamma_{zzz} + 2\gamma_{xxy} + 2\gamma_{xxz} + 2\gamma_{yyz}) \quad (16)$$

The delocalization energy ($E_{(2)}$), which represents interactions between donors (i) and acceptors (j), is given by the following equation:

$$E_{(2)} = q_i \frac{F(i, j)^2}{\epsilon_j - \epsilon_i} \quad (17)$$

(qi): the occupation of the donor orbital.

ϵ_i et ϵ_j : the diagonal elements (orbital energies).

F (i, j): the off-diagonal element of the Fock matrix.

Results and discussions

Optical egap calculation

The use of the result obtained from the UV-Vis spectrometric analysis spectrum is considered one of the most commonly used experimental methods for evaluating the optical properties of materials^{22,23}. It allows for the calculation of the values of allowed and forbidden direct or indirect transition gap energies. These energies represent the energy required to excite or move an electron from the valence band to the conduction band. In this regard, we use the Tauc method²⁴, in which we utilize the results of UV-Vis spectroscopy to study the variation of absorbed energy with the change in energy multiplied by the absorption coefficient α and the nature of the electronic transition γ , as shown in the following relation:

$$(\alpha h\nu)^\gamma = B (h\nu - E_{gap}) \quad (18)$$

α : absorption coefficient calculated directly with the Beer-Lumpe equation using the following relationship²⁵:

$$\alpha = \mathcal{A} (2.3026) \text{ cm}^{-1} \quad (19)$$

\mathcal{A} : absorbance.

h : Planck's constant.

ν : Photo's frequency.

E : Photon energy calculated with the wavelength by the relationship²⁶:

$$E = h\nu = \frac{h.c}{\lambda} \iff E = \frac{1240}{\lambda} \text{ (eV)} \quad (20)$$

B : proportionality constant.

E_{gap} : Dand gap energy.

γ : denotes the nature of the electronic transition.

$\gamma = 2$: direct allowed transitions.

$\gamma = \frac{2}{3}$: direct forbidden transitions.

$\gamma = \frac{1}{2}$: indirect allowed transitions.

$\gamma = \frac{1}{3}$: indirect forbidden transitions.

In the field of Second Harmonic Generation (SHG) nonlinear optics, we are interested in calculating the allowed direct bandgap transition, also referred to as the optical energy gap, as it is considered responsible for the creation or modification of a photon. To do this, we use the Tauc relationship with $\gamma = 2$, as presented in the following equation:

$$(\alpha h\nu)^2 = B (h\nu - E_{gap}) \quad (21)$$

The optical bandgap (E_{gap}) is measured using the linear portion of the graph of $(\alpha h\nu)^2$ as a function of $(h\nu)$ as shown in Fig. 8. The intersection of the line that includes the linear part of the curve with the x-axis represents the approximate value of the optical E_{gap} .

The obtained value of the optical E_{gap} is approximately 2.8 eV. This low value is attributed to the strong resonance and electron mobility π between the electron-donating dimethylamine and the strong electron-attracting nitro group. This result demonstrates that our compound (**n1**) exhibits very high Nonlinear Optical (NLO) behavior.

Structure properties

The results obtained after interpreting the X-ray diffraction data showed us that the **n1** crystals belong to the monoclinic system, using many programs that are used in analyzing and simulating the data, some of which were mentioned previously. The values of the obtained (**n1**) crystallographic information are represented in the following: $a = 8.7 \text{ \AA}$; $b = 17.73 \text{ \AA}$; $c = 14.07 \text{ \AA}$; $\alpha = \gamma = 90^\circ$; $\beta = 104.53^\circ$. With simulations by Match!3 software, certain crystallographic information can be summarized in the following Table 1.

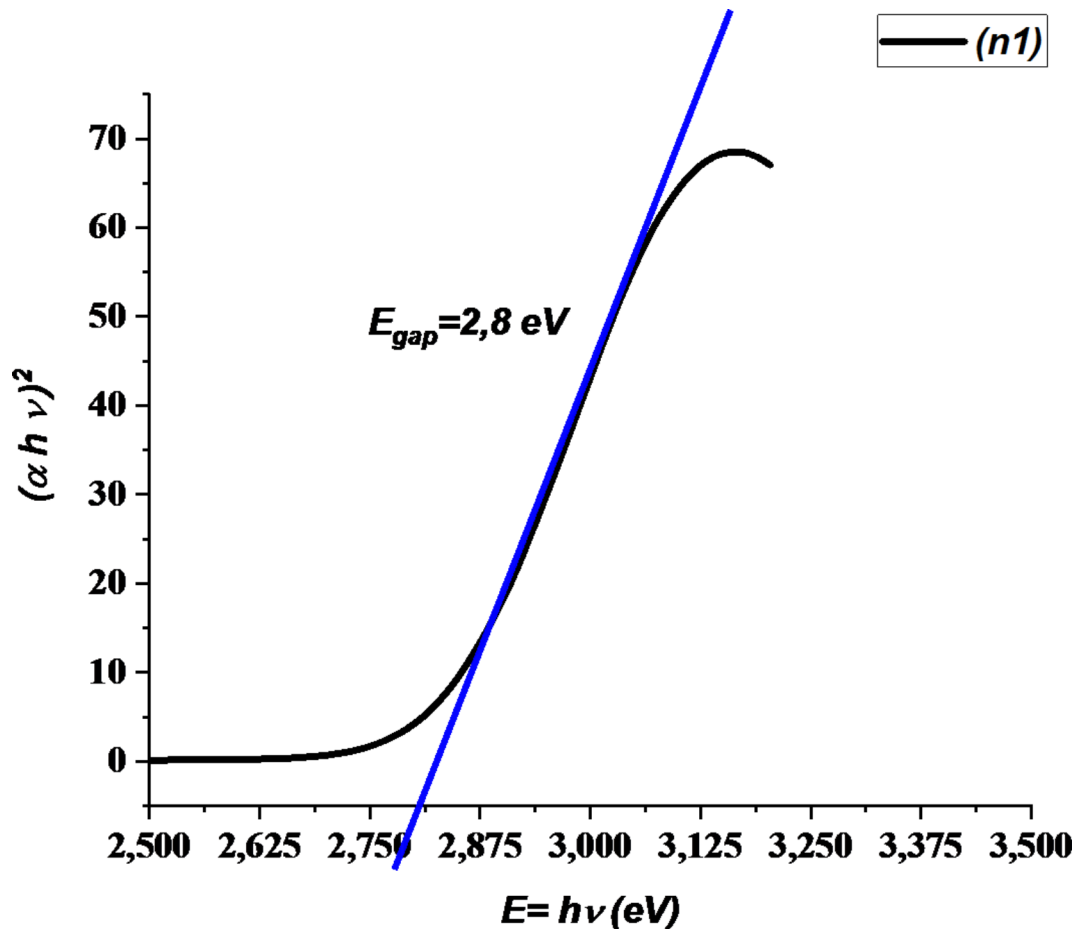


Fig. 8. Variation of $(\alpha h\nu)^2 = f(h\nu)$ and determination of E_{gap}

Parameters	Values
Chemical formula	C ₁₅ H ₁₅ N ₃ O ₂
Color and shape	Orange powder
Crystal structure	Monoclinic
Space group	14 : P121/c1, unique-b, cell-1
a	8.699410 Å
b	17.732713 Å
c	14.068079 Å
α = γ	90°
β	104.53°
Z	4
Z'	1000
Volume	V = 2100.789394 Å ³
Calculated density	d = 1.355 g cm ⁻³
Measurement range	3 – 90°

Table 1. Crystallographic data from our simulation on compound (n1).

Quantum DFT calculations

Selection of the functional

To identify the most suitable functional for experimental results, various families of functionals were evaluated using the 6-311++g(d,p) basis set for the molecule (n1) in two distinct states: gaseous (vacuum) and in a solvent medium (chloroform). This was carried out by spanning the entire spectrum of Hartree-Fock exchange

		CAM-B3lyp	LC-Blyp	LC-wPBE	B3lyp	M11	M062X
	$X_{\text{HF}} (\%)$	65	100	100	20	100	54
Vacuum	$E_{\text{gap}}^{\text{theo}}$ eV	3.155	7.67	7.534	5.521	7.29	5.17
Solvent Chloroforme	$E_{\text{gap}}^{\text{theo}}$ eV	2.70	7.29	7.4	5.06	6.74	4.79
	$E_{\text{gap}}^{\text{exp}}$ eV	2.8					
	$\Delta E_{\text{gap}} = E_{\text{gap}}^{\text{exp}} - E_{\text{gap}}^{\text{theo}} $	0.1	4.49	4.6	2.26	3.94	1.99

Table 2. Values of E_{gap} obtained using various functionals for functional selection. Significant values are in [bold].

n1		
Donor	Acceptor	$E_{(2)}$ Kcal mol ⁻¹
LP (1) (N ³)	π^* (C ⁶ -C ⁸)	59.81
π (C ⁶ -C ⁸)	π^* (C ⁷ -C ¹⁰)	43.02
π (C ⁷ -C ¹⁰)	π^* (C ¹⁴ -N ⁴)	27.68
LP (1) (N ⁴)	π^* (C ¹⁵ -C ¹⁷)	09.06
π (C ¹⁵ -C ¹⁷)	π^* (C ²⁰ -C ¹⁸)	28.96
π (C ¹⁸ -C ²⁰)	π^* (N ⁵ -O ²)	35.34

Table 3. Delocalization energies ($E_{(2)}$) calculated using CAM-B3LYP/6-311++G(d,p). Significant values are in [bold].

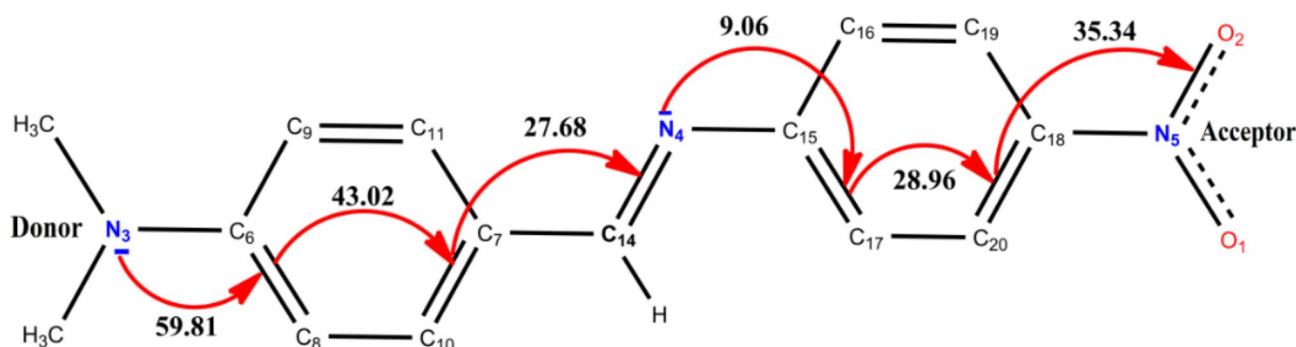


Fig. 9. Donor to acceptor trajectory (n1).

percentages, ranging from 0 to 100%. The considered functionals encompassed global hybrids like B3LYP, M06-2X, as well as hybrid functionals such as CAM-B3LYP (Coulomb-attenuated). Each of these functionals featured a fixed amount of exact exchange, as indicated respectively in Table 1 below, to investigate the impact of exchange on the energy gap. The experimental value of the gap ($E_{\text{gap}}^{\text{exp}}$) served as a benchmark for selecting the value closest to the theoretically computed energy gap achieved using the different functionals as presented in Table 2.

Based on the obtained results, it is clearly observed that the closest value to the experimental E_{gap} is 2.7 eV, obtained with CAM-B3LYP, in contrast to other functional that yield values significantly distant from $E_{\text{gap}}^{\text{exp}}$. It can be observed that the CAM-B3LYP functional provides the E_{gap} value closest to the experimental one. Our findings align with other studies conducted for functional selection²⁷. In the subsequent phases of our work, we utilized the CAM-B3LYP functional in combination with the 6-311++g(d,p) basis set.

NBO analysis

This section focuses on the determination of delocalization energies $E_{(2)}$ calculated using the NBO method, as expressed in Eq. (17), to describe the mechanism of Intramolecular Charge Transfer (ICT) between the Donor (D) and Acceptor (A) and their trajectories within the molecule (n1). The corresponding results are presented in Table 3. It should be noted that the atom numbering in the structures reported in Table 2 was assigned by the visualization software Gaussview05.

Figure 9 illustrates the mechanism of intramolecular charge transfer and the delocalization pathway created by the interaction between the attractor and the donor within molecule (n1).

According to Fig. 8, it is noteworthy that the Intramolecular Charge Transfer (ICT) in molecule (n1) is oriented from the dimethylamino group towards the nitro group. This is explained by the attractive effect

between the acceptor and the donor. The lone pairs of nitrogen atoms carried by dimethylamino as the donor and the nitrogen of the imine (N4=C14) contribute to the ICT pathway. Based on the results, molecule (**n1**) has maintained electronic conjugation along the electron chain, as evidenced by significant delocalization energy values. The continuity of this delocalization along the chain explains the strong attraction created by the acceptor on the donor, giving this molecule a highly polarizable “push-pull” character. Furthermore, it can be concluded that this type of molecule can provide a nonlinear optical response in a specific direction created by the two D-A poles, confirming that our molecule is non-centrosymmetric and therefore highly recommended for consideration as an active system in nonlinear optics (NLO).

The $E_{(2)}$ energies provided by the double bonds all fall within the range of 27 to 43 Kcal.mol⁻¹, and the $E_{(2)}$ energies provided by the lone pairs (LP) of nitrogen (N3 and N4) are in the range of 9 to 59 Kcal mol⁻¹. This can be explained by the significant contribution of the nitrogen lone pair (LP) as an electron donor. From these observations, it can be concluded that the ICT mechanism in molecule (**n1**) is characterized by a well-defined direction: Donor to Acceptor. This phenomenon is in good agreement with the Forster approach^{28,29}.

Linear and nonlinear optical parameters

In this section, a theoretical study was conducted on our molecule (**n1**) to evaluate its activity in the field of nonlinear optics (NLO). A key parameter used to justify the effectiveness of a material in NLO is the first-order hyperpolarizability (β), which is the second derivative of the dipole moment. Its non-zero value confirms that the material is non-centrosymmetric.

Linear (LO) and nonlinear optical (NLO) parameters were determined in this section using the CAM-B3LYP/6-311++g(d,p) functional. The objective of the study is to describe the variation of the aforementioned parameters in static and dynamic states during second harmonic generation (SHG) at different wavelengths. These various values characterize the incident waves of lasers, which were obtained from several previous works³⁰. The results are reported in Table 3.

Table 4 represents the values of total dipole moments (μ_{tot}), static isotropic polarizabilities (α^∞), dynamic polarizabilities (α^λ), static and dynamic anisotropic polarizabilities ($\Delta\alpha^{\lambda \neq \infty}$), first hyperpolarizability (β_{tot}), and second hyperpolarizability (third harmonic generation THG) (γ) calculated at various wavelengths (eV and nm).

the calculated values have been converted into electrostatic units (esu) (α : 1 a.u.=0.1482 $\times 10^{-24}$ esu; β : 1 a.u.=8.6393 $\times 10^{-33}$ esu).

From the results obtained in Table 4, it can be seen that the values of the linear and nonlinear properties of (**n1**) compound are very close when the wavelength is greater than 1062 nm. This means that compound does not show any change in its linear or nonlinear optical properties and the light processing by this material is almost uniform. We notice that for the wavelength at 1062 nm and 720 nm, there is a change in most of the values of the linear and nonlinear properties. First, the static and dynamic azeotropic polarization ($\Delta\alpha$) increased from 51.8×10^{-24} to 57.55×10^{-24} esu, which may lead to a change in the refractive index of this material or a change in its polarization³¹. Secondly, the increase in the first hyperpolarizability (β_{tot}) values, which went from 117.9×10^{-30} to 160.08×10^{-30} esu, shows an increase in the nonlinear response of the (**n1**), which makes it of particular interest in applications using nonlinear effects such as nonlinear scattering, second harmonic generation (SHG) and in communication systems^{32,33}. Finally, the significant change in the obtained values concerns the second hyperpolarizability (γ) values, which went from 62.28×10^{-35} esu at $\lambda = 1064$ nm to 4227.1×10^{-35} esu at $\lambda = 720$ nm. This indicates a nonlinear response of the **n1** material to third harmonic generation (THG)^{34–36}.

Global reactivity parameters

Electronic transition parameters were calculated using Time-Dependent Density Functional Theory (TD-DFT) with the CAM-B3LYP/6-311++g(d,p) functional. The objective is to evaluate the excited states of molecule (**n1**) to more accurately analyze the nature of electronic transitions within our molecule in the gas phase (vacuum).

The results in Table 5 are consistent with the previous experimental and theoretical findings. The dipole moment of molecule (**n1**) is high with a low E_{gap} . This indicates a significant charge transfer within the system of our molecule (**n1**). Figure 10 depicts the frontier orbitals of molecule (**n1**) obtained using the TDA-CAM-B3LYP/6-311g(d,p) functional.

According to Fig. 10, it is evident that all electron densities in both vacuum and solvent environments are nearly identical. This indicates that these orbitals are minimally affected by the solvent effect. The electron density of the Highest Occupied Molecular Orbital (HOMO) surrounds almost the entire molecule in both cases, with virtually no density on the acceptor group ($-\text{NO}_2$). In contrast, the electron density of the Lowest Unoccupied

Settings	0.00 eV ($\lambda = \infty$)	0.25 eV (4959 nm)	0.50 eV (2479 nm)	0.65 eV (1907 nm)	0.85 eV (1550 nm)	1.16 eV (1064 nm)	1.72 eV (720 nm)
μ_{tot} Debye	11.93	–	–	–	–	–	–
$\Delta\alpha \cdot 10^{-24}$ esu	46.86	47.03	47.57	48.08	48.74	51.08	57.55
$\alpha \cdot 10^{-24}$ esu	38.76	38.83	39.04	39.25	39.51	40.43	42.92
$\beta_{tot} \cdot 10^{-30}$ esu	94.23	95.11	97.98	100.73	104.36	117.91	160.08
$\gamma \cdot 10^{-35}$ esu	21.96	22.82	25.66	28.76	33.55	62.28	4227.10

Table 4. NLO parameters calculated with CAM-B3LYP/6-311++g(d,p).

Settings	E_H	E_L	E_{gap}	EI	AE	η	χ	μ_{tot}
Values	-5.782	-2.616	3.166	5.782	2.216	1.583	4.19	12.02
Unit	eV							Debye

Table 5. Global reactivity parameters, μ_{tot} in Debye, the remaining parameters in eV.

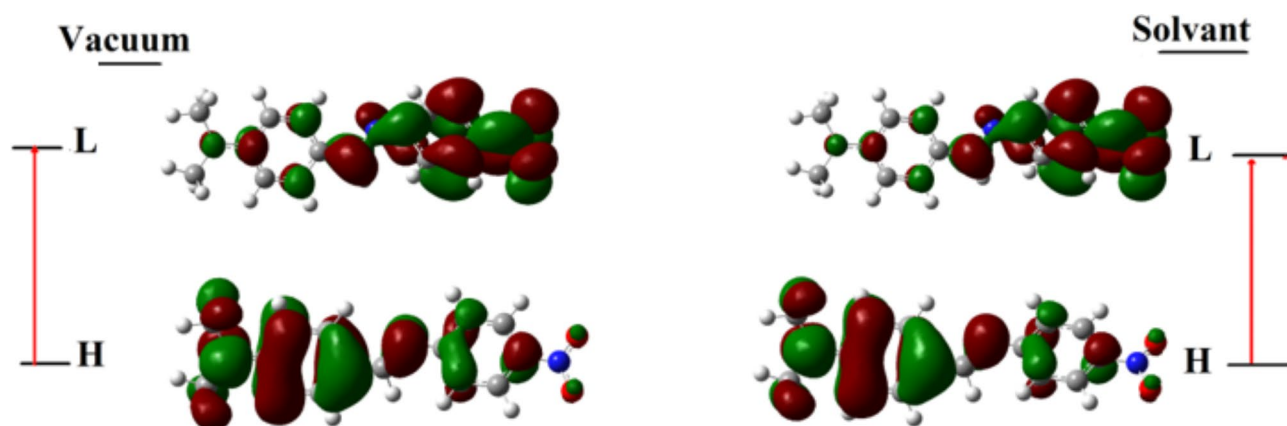


Fig. 10. Frontier orbitals of (**n1**) in vacuum and in solvent.

Molecular Orbital (LUMO) is distributed over the entire molecule, including the acceptor group. Thus, the HOMO-LUMO excitation shifts from the donor group to the acceptor group, confirming the NBO theory (ICT trajectory). Furthermore, the HOMO orbital is of (n) type, and the LUMO orbital is of π^* type. Therefore, it is likely that the HOMO \rightarrow LUMO excitation is of the $n \rightarrow \pi^*$ type, which is attributed to the significant contribution of the donor's lone pair (LP).

Conclusion

This work was conducted through a combination of experimental and theoretical studies, involving multiple aspects including synthesis, spectroscopic analyses, optical energy gap measurement, and theoretical investigations. Compound (**n1**) represents a novel non-centrosymmetric Schiff base derivative, synthesized with a very acceptable yield in a single step. The molecular structure of (**n1**) was confirmed through various spectroscopic analyses such as FT-IR, NMR ^1H , and ^{13}C . To assess the potential of our compound (**n1**) in nonlinear optics, we employed the Tauc method, utilizing UV-visible analysis data along with quantum chemical calculations using Gaussian09. The optical energy gap (E_{gap}) of (**n1**), calculated using the Tauc method, is determined to be 2.7 eV. The theoretical studies demonstrated that the CAM-B3LYP functional is the most reliable for our research, as it yields an E_{gap} value closest to the experimental one. Compound (**n1**) exhibits strong intramolecular electronic exchange, as evidenced by the high values of dipole moments (μ) and hyperpolarizabilities (β). The linear and nonlinear optical properties of our compound are summarized by parameters such as $\Delta\alpha$, α , and the hyperpolarizabilities (β_{tot}), (γ_{tot}), both static and dynamic, which showed a response strongly dependent on the incident wavelength. Based on the increasing of the first superpolarization (β_{tot}) values from 1064 to 720 nm, which showed a significant variation, it reflects improvements in the nonlinear properties of the material (**n1**). This may be useful in improving performance in devices that rely on nonlinear effects, such as nonlinear optical material converter, optical switch, or optical components in communications systems. These studies on compound (**n1**) confirm its promising performance in the field of nonlinear optics. In future work, modifications to the structure of (**n1**) will be explored with the aim of enhancing its properties.

Data availability

The datasets generated and/or analyzed during the current study are available in repository fid, GaussView, excel and origin files.

Received: 5 June 2024; Accepted: 1 October 2024

Published online: 09 November 2024

References

- Han, D. et al. Nanosecond resolution photography system for laser-induced cavitation based on PIV dual-head laser and industrial camera. *Ultrason. Sonochem.* **78**, 105733. <https://doi.org/10.1016/j.ultsonch.2021.105733> (2021).
- Mariana, C. C., Vázquez-Lepe, E., Martínez-López, J. I., Rodríguez, C. A. & García-López, E. Influence of process parameters on surface topography of nitinol manufactured by fiber laser cutting for medical applications. *Procedia CIRP* **110**, 82–86. <https://doi.org/10.1016/j.procir.2022.06.017> (2022).

3. Wang, J. et al. High-precision dynamic pointing method for improving the acquisition performance of laser communication between high-altitude platform stations. *Optik* **275**, 170621. <https://doi.org/10.1016/j.jleo.2023.170621> (2023).
4. Wang, J., Song, Y., Jiang, H., Dong, K. & Liu, Y. High-precision dynamic pointing method for improving the acquisition performance of laser communication between high-altitude platform stations. *Optik* **274**, 170552. <https://doi.org/10.1016/j.jleo.2023.170552> (2023).
5. Muric, B. D., Pantelic, D. V., Vasiljevic, D. M., Savic-Sevic, S. N. & Jelenkovic, B. M. Application of tol'hema eosin sensitized gelatin as a potential eye protection filter against direct laser radiation. *Curr. Appl. Phys.* **16**, 57–62. <https://doi.org/10.1016/j.cap.2015.09.014> (2016).
6. Abdel-Rahman, L. H., Abu-Dief, A. M., Moustafa, H. & Abdel-Mawgoud, A. A. H. Design and nonlinear optical properties (NLO) using DFT approach of new Cr (III), VO (II), and Ni (II) chelates incorporating tri-dentate imine ligand for DNA interaction, antimicrobial, anticancer activities and molecular docking studies. *Arab. J. Chem.* **13**, 649–670. <https://doi.org/10.1016/j.arabjc.2017.07.007> (2020).
7. Ceylan, Ü., Çapan, A., Yalçın, Ş. P., Sönmez, M., & Aygün, M. Vibrational spectroscopic and thermo dynamical property studies, Fukui functions, HOMO-LUMO, NLO, NBO and crystal structure analysis of a new Schiff base bearing phenoxy-imine group. *J. Mol. Struct.* **1136**, 222–230. <https://doi.org/10.1016/j.molstruc.2017.02.014> (2017).
8. Maza, S. et al. Synthesis, structural investigation and NLO properties of three 1, 2, 4-triazole Schiff bases. *J. Mol. Struct.* **1219**, 128492. <https://doi.org/10.1016/j.molstruc.2020.128492> (2020).
9. Şahin, S. & Dege, N. Synthesis, characterization, X-ray, HOMO-LUMO, MEP, FT-IR, NLO, Hirshfeld surface, ADMET, boiled-egg model properties and molecular docking studies with human cyclophilin D (CypD) of a Schiff base compound:(E)-1-(5-nitro-2-(piperidin-1-yl) phenyl)-N-(3-nitrophenyl) methanimine. *Polyhedron* **205**, 115320. <https://doi.org/10.1016/j.poly.2021.115320> (2021).
10. Roufieda Guerroudj, A. et al. Synthesis, crystal structure, vibrational spectral investigation, intermolecular interactions, chemical reactivity, NLO properties and molecular docking analysis on (E)-N-(4-nitrobenzylidene)-3-chlorobenzenamine: A combined experimental and theoretical study. *J. Mol. Struct.* **1240**, 130589. <https://doi.org/10.1016/j.molstruc.2021.130589> (2021).
11. Balachandrar, R. K. & Kalainathan, S. Synthesis, crystal growth and spectroscopic investigation of second order organic nonlinear optical single crystal: 2-Chloro-N-[4-(dimethylamino) benzylidene] aniline. *Spectrochim. Acta Part A: Mol. Biomol. Spectrosc.* **116**, 143–147. <https://doi.org/10.1016/j.saa.2013.07.021> (2013).
12. Leela, S., Hema, R., Stoeckli-Evans, H., Ramamurthi, K. & Bhagavannarayana, G. Design, synthesis, growth and characterization of 4-methoxy-4'-dimethylamino-benzylidene aniline (MDMABA): a novel third order nonlinear optical material. *Spectrochim. Acta Part A: Mol. Biomol. Spectrosc.* **77**, 927–932. <https://doi.org/10.1016/j.saa.2010.08.012> (2010).
13. Pandey, P. & Rai, R. N. Synthesis and studies on structural, optical and nonlinear optical properties of novel organic intermolecular compounds: 4-chloro-3-nitroaniline– 3-hydroxy benzaldehyde and urea– 4-dimethylaminopyridine. *J. Mol. Struct.* **1160**, 189–197. <https://doi.org/10.1016/j.molstruc.2018.02.002> (2018).
14. Ünver, H., Karakas, A. & Elmali, A. Nonlinear optical properties, spectroscopic studies and structure of 2-hydroxy-3-methoxy-N-(2-chloro-benzyl)-benzaldehyde-imine. *J. Mol. Struct.* **702**, 49–54; <https://doi.org/10.1016/j.molstruc.2004.06.008> (2004).
15. Ojo, N. D., Krause, R. W. & Obi-Egbedi, N. O. Electronic and nonlinear optical properties of 3-((2-substituted-4-nitrophenyl) imino) methyl phenol. *Comput. Theor. Chem.* **1192**, 113050. <https://doi.org/10.1016/j.comptc.2020.113050> (2020).
16. Salihi, K. S. M. Synthesis, characterization, surface analysis, optical activity and solvent effects on the electronic absorptions of Schiff base-functionalized amino thiophene derivatives: Experimental and TD-DFT investigations. *J. Mol. Struct.* **1244**, 131267. <https://doi.org/10.1016/j.molstruc.2021.131267> (2021).
17. Man, L.-M. et al. Synthesis, crystal structure, vibrational spectra, nonlinear optical property of an organic charge-transfer compound—4-nitrobenzyl isoquinolinium picrate based on DFT calculations. *J. Mol. Struct.* **1175**, 971–978. <https://doi.org/10.1016/j.molstruc.2018.07.054> (2019).
18. Saha, A., Shukla, V., Choudhury, S. & Jayabalan, J. Design, synthesis and nonlinear optical properties of (E)-1-(4-substituted)-3-(4-hydroxy-3-nitrophenyl) prop-2-en-1-one compounds. *Chem. Phys. Lett.* **653**, 184–189. <https://doi.org/10.1016/j.cplett.2016.04.084> (2016).
19. Lei, Y. et al. Synthesis, growth and mechanical properties of mid-infrared nonlinear optical crystal CdGeAs₂. *J. Crystal Growth* **562**, 126060. <https://doi.org/10.1016/j.jcrysgro.2021.126060> (2021).
20. Tauc, J., Grigorovici, R. & Vancu, A. Optical properties and electronic structure of amorphous germanium. *Phys. Status Solidi, B* **15**(2), 627–637. <https://doi.org/10.1002/pssb.19660150224> (1966).
21. Soltani, N. et al. Visible light-induced degradation of methylene blue in the presence of photocatalytic ZnS and CdS nanoparticles. *Int. J. Mol. Sci.* **13**(10), 12242–12258. <https://doi.org/10.3390/ijms131012242> (2012).
22. Pramod, A. G., Nadaf, Y. F. & Renuka, C. G. Synthesis and structural characterization via spectroscopic techniques of a novel compound derived from methanimine, along with the evaluation of its linear and nonlinear optical properties using quantum chemistry. *J. Mol. Struct.* **1194**, 271–283. <https://doi.org/10.1016/j.molstruc.201905099> (2019).
23. Khelladi, I., Springborg, M., Rahmouni, A., Chadli, R. & Sekkal-Rahal, M. Theoretical study on non-linear optics properties of polycyclic aromatic hydrocarbons and the effect of their intercalation with carbon nanotubes. *Molecules* **28**, 110. <https://doi.org/10.3390/molecules28010110> (2023).
24. Dogan, F., Temizkan, K. & Kaya, I. A novel shape-controlled synthesis of bifunctional organic polymeric nanoparticles. *Polymer* **70**, 59–67. <https://doi.org/10.1016/j.polymer.2015.06.007> (2015).
25. Förster, T. Zwischenmolekulare energiewanderung und fluoreszenz. *Ann. Phys.* **2**, 55–75. <https://doi.org/10.1002/andp.19484370105> (1948).
26. Förster, T. *Modern Quantum Chemistry, Istanbul Lectures. Part III* 93–137 (Academic Press, 1965).
27. Shalin, N. I., Fominykh, O. D. & Balakina, M. Y. Synthesis and structural characterization via spectroscopic techniques of a novel compound derived from methanimine, along with the evaluation of its linear and nonlinear optical properties using quantum chemistry. *Chem. Phys. Lett.* **717**, 21–28. <https://doi.org/10.1016/j.cplett.2018.12.045> (2019).
28. Marcano, E., Squitieri, E., Murgich, J. & Soscún, H. Theoretical investigation of the static (dynamic) polarizability and second hyperpolarizability of DAAD quadrupolar push–pull molecules. A comparison among HF (TD-HF), DFT (TD-B3LYP), and MP2 (TD-MP2) methods. *Comput. Theor. Chem.* **985**, 72–79. <https://doi.org/10.1016/j.comptc.2012.02.001> (2012).
29. Sahraoui, B., Rivoire, G., Terkia-Derdra, N., Salle, M. & Zaremba, J. Third-order nonlinear optical properties of new bisdithiafulvenyl-substituted tetrathiafulvalene. *J. Opt. Soc. Am. B* **15**, 923–28. <https://doi.org/10.1364/JOSAB.15.000923> (1998).
30. Zongo, S. et al. Nonlinear optical properties of poly (methyl methacrylate) thin films doped with Bixa Orellana dye. *Appl. Surface Sci.* **340**, 72–77. <https://doi.org/10.1016/j.apsusc.2015.02.161> (2015).
31. Guezguez, I. et al. Zinc induced a dramatic enhancement of the nonlinear optical properties of an azo-based iminopyridine ligand. *J. Phys. Chem. C* **118**, 7545–7553. <https://doi.org/10.1021/jp412204f> (2014).
32. Karthick, S. et al. Synthesis, structural, dielectric, laser damage threshold, third order nonlinear optical and quantum chemical investigations on a novel organic crystalline material: pyrrolidin-1-ium 2-chloro-4-nitrobenzoate 2-chloro-4-nitrobenzoic acid for opto-electronic applications. *Opt. Laser Technol.* **122**, 1058492. <https://doi.org/10.1016/j.optlastec.2019.105849> (2020).
33. Sahraoui, B., Nguyen Phu, X., Salle, M. & Gorgues, A. Electronic and nuclear contributions to the third-order nonlinear optical susceptibilities of new pN, N'-dimethylaniline tetrathiafulvalene derivatives. *Opt. Lett.* **23**, 1811–1813. <https://doi.org/10.1364/OE.23.001811> (1998).

34. Zawadzka, A., Płóciennik, P., Strzelecki, J., Lukasiak, Z. & Sahraoui, B. Photophysical properties of Alq3 thin films. *Opt. Mater.* **36**, 91–97. <https://doi.org/10.1016/j.optmat.2013.05.001> (2014).
35. Bouchouit, K. et al. Experimental and theoretical studies of NLO properties of organic–inorganic materials base on p-nitroaniline. *Chem. Phys. Lett.* **455**, 270–274. <https://doi.org/10.1016/j.cplett.2008.02.101> (2008).
36. Kulyk, B., Guichaoua, D., Ayadi, A., El-Ghayoury, A. & Sahraoui, B. Functionalized azo-based iminopyridine rhenium complexes for nonlinear optical performance. *Dyes Pigments* **145**, 256–262. <https://doi.org/10.1016/j.dyepig.2017.06.012> (2017).

Acknowledgements

The authors send their sincere thanks and greetings to the Directorate of Scientific Research in the first place and to all the laboratories which participated in the success of this work. The financial support for this scientific research was provided by the laboratory chemical physic, organic and macromolecules (LCPOM), department of chemistry, faculty of exacts sciences, university Djillali LIABES, Sidi Bel Abbes, Algeria.

Author contributions

R. CHADLI, I. KHELLADI, B. AMERI are concerned with the organic synthesis part and the spectroscopic analyzes and M. Zouaui Rabeh with A. HADDOU are responsible for the theoretical calculations. both teams are supervised by Pr M. SAKKAL-RAHAL.

Funding

The financial support for this scientific research was provided by faculty of exacts sciences, university Djillali LIABES, Sidi Bel Abbes, Algeria.

Competing interests

The authors declare no competing interests.

Additional information

Supplementary Information The online version contains supplementary material available at <https://doi.org/10.1038/s41598-024-75117-6>.

Correspondence and requests for materials should be addressed to R.C.

Reprints and permissions information is available at www.nature.com/reprints.

Publisher's note Springer Nature remains neutral with regard to jurisdictional claims in published maps and institutional affiliations.

Open Access This article is licensed under a Creative Commons Attribution-NonCommercial-NoDerivatives 4.0 International License, which permits any non-commercial use, sharing, distribution and reproduction in any medium or format, as long as you give appropriate credit to the original author(s) and the source, provide a link to the Creative Commons licence, and indicate if you modified the licensed material. You do not have permission under this licence to share adapted material derived from this article or parts of it. The images or other third party material in this article are included in the article's Creative Commons licence, unless indicated otherwise in a credit line to the material. If material is not included in the article's Creative Commons licence and your intended use is not permitted by statutory regulation or exceeds the permitted use, you will need to obtain permission directly from the copyright holder. To view a copy of this licence, visit <http://creativecommons.org/licenses/by-nc-nd/4.0/>.

© The Author(s) 2024